Available online at www.sciencedirect.com
SCIENCE DIRECT
Journal of Solid State Chemistry 179 (2006) 1060–1066
JOURNAL OF SOLID STATE CHEMISTRY
www.elsevier.com/locate/jssc

Thioether moiety functionalization of mesoporous silica films for the encapsulation of highly dispersed gold nanoparticles

Jinlou Gu, Liangming Xiong, Jianlin Shi*, Zile Hua, Lingxia Zhang, Lei Li

State Key Lab of High Performance Ceramics and Superfine Microstructure, Shanghai Institute of Ceramics, Chinese Academy of Sciences, Shanghai 200050, People's Republic of China

Received 18 October 2005; received in revised form 22 December 2005; accepted 1 January 2006
Available online 30 January 2006

Abstract

Highly dispersed gold nanoparticles within mesoporous thin films (MTFs) have been synthesized through a newly developed controllable strategy, in which (1,4)-*bis*(triethoxysilyl)propane tetrasufide (BPTS) organosiloxane coupling agent was co-assembled with tetraethyl orthosilicate (TEOS) to form organic groups functionalized mesoporous composite films followed with oxidization, ion-exchange with $Au(en)_2Cl_3$ (en: 1,2-ethanediamine) compound and calcination under hydrogen/nitrogen mixing atmosphere. Small-angle X-ray diffraction (XRD) characterization indicated that up to 10 mol% of BPTS could be incorporated into mesoporous hybrid films, and that would not breakup the structural integrity and long-range periodicity. The loaded gold nanoparticles were uniformly distributed due to the molecular level homogenous mixing of the BPTS precursor with TEOS, and its concentration could be controlled via the original ratio of BPTS to TEOS. The nanoparticles had a narrow size distribution with diameters in the size range of 3–7 nm through transmission electron microscopy (TEM) observation and underwent a slight size increase with the higher gold load level. An overall increase in the absorption intensity, a red shift of absorption peak, together with a comparatively narrower bandwidth could be observed at higher gold concentration within composite films from UV–vis spectra. Wide-angle XRD, TEM, X-ray photoelectron spectroscopy (XPS) and UV–vis spectra characterizations all agreed on the fact that the gold loading level could be controlled by the amount of BPTS in the starting sol for preparing MTFs.

Keywords: Mesoporous thin films; Silica; Gold nanoparticles; Host–guest assembly

1. Introduction

Composite films containing metal nanoparticles have been the focus of many researchers due to their current and potential applications in the fields of photochemistry, biosensors, nonlinear optics as well as their fundamental scientific significance [1–5]. Numerous physical and chemical methods have been successfully employed to fabricate these kinds of composite films, including ion implantation [6], sputtering [7], sol–gel process [8], and their combinations [9]. Although homogeneously dispersed metal nanoparticles could be obtained in the films from some of those fabrication methods [10,11], the development of alternative preparation routes that allow for the production of metal nanoparticle with uniform size, high dispersion, and controllable concentration is still desirable.

Recently, periodic mesoporous materials, synthesized via the polymerization of inorganic silica around organic template [12,13], have been used as molds for the growth of different metals with controlled size and morphology, which provided an ideal route to optimize the space filling with nanoparticles in a solid porous matrix [14–20]. In fact, due to the easy control of macroscopic morphology of the mesoporous material, the mesoporous silica thin films are very facile to prepare and easy to be integrated into the existing structures such as waveguides to meet the practical optical needs [5,21]. However, up to date, the preparation of metallic nanoparticles within mesoporous thin films (MTFs) has not been well explored [22–24]. Most attempts have been centered on aqueous impregnation methods, which are somewhat limited by the tendency of metallic

*Corresponding author. Fax: +86 21 52412833.
E-mail address: jlshi@sunm.shcnc.ac.cn (J. Shi).

0022-4596/$ - see front matter © 2006 Elsevier Inc. All rights reserved.
doi:10.1016/j.jssc.2006.01.002

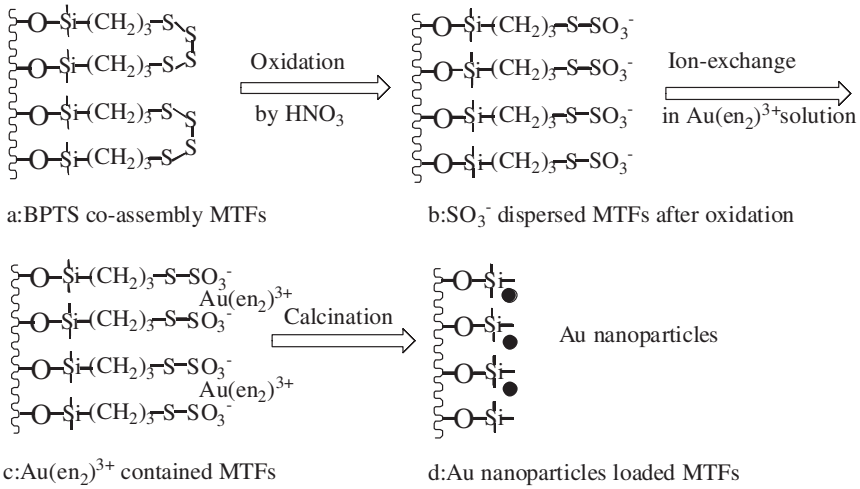

Scheme 1. Proposed mechanism for the formation of Au nanoparticles embedded composite films. (a) BPTS co-assembly MTFs, (b) SO_3^- dispersed MTFs after oxidation, (c) $Au(en_2)^{3+}$ contained MTFs, and (d) Au nanoparticles loaded MTFs.

nanoparticles to agglomerate on the outside surface of MTFs [25]. In addition, wet impregnation process is time consuming [26] and could not be used to introduce controllable amount of metal precursors since it is dependent on the charge of the silica matrix [27]. Functionalization of the mesoporous silica with charged groups via postsynthesis grafting or co-condensation method to enhance the interaction between metal complex precursors and silica surface seems to be an efficient strategy to incorporate or dope metal nanoparticles in mesoporous materials [28,29]. However, the postsynthesis grafting method typically results in inhomogeneous inner surface coverage because the introduced organic charged moieties congregate near the entries to the mesoporous channels. Therefore, the resultant incorporated metal nanoparticles could not be uniformly distributed within MTFs [30]. Furthermore, the key drawback of this method is difficult to control over the concentration of grafted organic group since its grafted amount is dependent on the number of free Si–OH bonds on the inner pore surface of MTFs as our group [31] and the other group demonstrated [32]. In our previous work, it was found that BPTS ($(CH_3CH_2O)_3Si(CH_2)_3S$–S–S–$S(CH_2)_3Si(OCH_2CH_3)_3$) was facile to be co-assembled into the framework of mesoporous molecular sieves, and the co-assembly amount of BPTS was controllable [33]. Moreover, BPTS was easy to be oxidized to form $-SO_3^-$ bearing anionic compounds [34], which would effectively enhance the interaction with cationic complex such as $Au(en)_2^{3+}$. Since this co-condensation method is based on the molecular level mixing of BPTS with tetraethyl orthosilicate (TEOS), the thioether bearing organosiloxane of BPTS could be uniformly distributed in the framework of MTFs [35].

Herein, we developed a new ion-exchange method for the incorporation of controllable amount of $Au(en)_2^{3+}$ into MTFs functionalized with $-SO_3^-$ group which was introduced from the co-condensation reaction of BPTS with TEOS in a template environment. The synthesis route is shown in Scheme 1. Controllable amount of BPTS compounds were first co-assembled into the mesoporous wall of MTFs. After oxidation with concentrated HNO_3, $-SO_3^-$ groups were uniformly dispersed within MTFs [34]. Following with ion-exchange, a variety of metal cationic complex, such as $Au(en)_2^{3+}$ in this study, could be introduced into MTFs in a short time. Finally, MTFs loaded with controllable amount of gold nanoparticles could be obtained after the calcinations of composite films under hydrogen and nitrogen (with H_2 molar ratio of 5%) mixing atmosphere [36].

2. Experimental section

2.1. Preparation of composite films

In the current investigation, using Brij56 ($CH_3(CH_2)_{15}(EO)_{10}OH$, Fluka) as templates, samples were synthesized by the one-step co-condensation of TEOS (98%, Aldrich) with different proportions of BPTS (Acros Organics). Typically, $0.03435\times(1-2x)$ (when $x=0$, it is 7.68 mL) mol of TEOS were prehydrolyzed in a solution containing 3.71 g of dilute hydrochloric acid ($pH\approx 2$, isoelectric point of silica) and 10 mL of tetrahydrofuran (THF) under vigorous stirring at room temperature. A few minutes later, $0.03435x$ mol of BPTS was added. Following stirring for 120 min, this prehydrolyzed precursor solution was mixed with a solution containing 2.33 g of Brij56 dissolved in 30 mL of THF. The resultant solution was further stirred for 15 min. From this mixture with a final molar composition of TEOS:BPTS:Brij:H_2O:HCl:THF $=(1-2x):x$:0.0994:5:0.0090:25, thin films were prepared by dip-coating onto cleaned glass slides at 75 mm min^{-1}, where $x=0$, 0.02, 0.04, 0.06, 0.08 and 0.10 corresponding to BPTS molar ratio of 0%, 2%, 4%, 6%, 8% and 10% to TEOS, respectively. The films were stored at room temperature for 24 h and then extracted using ethanol with a little HCl (37%) being added under refluxed

condition to remove the Brij56 surfactant. The resultant films were extensively washed with ethanol and deionized water and denoted as S0, S2, S4, S6, S8, S10 corresponding to the BPTS molar concentrations of 0%, 2%, 4%, 6%, 8% and 10%, respectively. It should be kept in mind that 1 mol of BPTS contained 2 mol of $-S-S-(CH_2)_3Si(OCH_2CH_3)_3$ moiety, which meant that if 10 mol% of BPTS was co-condensed into the MTFs, 20 mol% negative charged groups of SO_3^- could be obtained. The resultant films were dipped into concentrated HNO_3 (63%) solution for 3–5 min and then washed with de-ionized water for several times. Subsequently, $-SO_3^-$ bearing composite films were dipped into 0.05 M $Au(en)_2Cl_3$ aqueous solution, which was synthesized according to the literature [37]. Because the electrostatic interaction between anionic SO_3^- and cationic complex of $Au(en)_2^{3+}$ was very strong, mixing for ca. 5 min was sufficient to have fully ion-exchange samples. The resultant films were washed with copious amounts of ethanol, dried in ambient air and then reduced at 300 °C for 2 h under hydrogen and nitrogen mixing atmosphere to obtain the gold nanoparticles loaded MTFs.

2.2. Characterizations

Fourier transformation infrared (FT-IR) spectra were conducted using a Nicolet 7000-C spectroscopy with 4 cm^{-1} resolutions. The samples were prepared by scratching the films off the substrate and dispersed in KBr pellets. X-ray diffraction (XRD) patterns were collected with Rigaku D/MAX-2200PC X-ray diffractometer using Cu$K\alpha$ radiation (40 kV, 40 mA $\lambda = 1.5418$ Å). Transmission electron microscopy (TEM) images, selected area electron diffraction (SAED) patterns and energy dispersive spectrum (EDS) were performed with a JEOL 200CX electron microscope equipped with an Oxford EDS analysis system operated at 200 kV. The TEM samples were prepared by scratching the film off the substrate, dispersed the scraps in ethanol, and deposited them onto a holey carbon film on a Cu grid. UV–vis absorption spectra were recorded on a Shimadzu UV–vis 3101 spectroscopy. X-ray photoelectron spectroscopy (XPS) analysis was performed on a VG Microlab MK-II (Mg$K\alpha$ 300 W) system. Calibration of the binding energies was made with the C1*s* binding energy of standard hydrocarbons (284.6 eV).

3. Results and discussion

The assembly process was monitored with FT-IR and XPS spectra. Fig. 1 shows FT-IR spectra of MTFs without any BPTS as well as the co-assembled MTFs. The disappearance of the IR absorption at 2900–3000 cm^{-1} assigned to C–H bonds after the extraction using ethanol with a slight of HCl indicates that the surfactant has been removed from the MTFs as shown in Fig. 1a. However, when BPTS is co-assembled with TEOS, strong absorption at 2900–3000 cm^{-1} can be clearly observed before extraction, and after extraction, these kinds of absorption peaks are preserved with reduced relative intensity which should be originated from the C–H bonds in BPTS [31]. These results indicate that BPTS has been successfully introduced into MTFs, which will provide thioether bonds for further oxidation to form negatively charged $-SO_3^-$ groups. Fig. 2 shows XPS spectra of co-condensed MTFs samples of S4 before (a) and after (b) oxidation with concentrated HNO_3. A peak with binding energy of 163.3 eV is observed for S2*p* electron of the pristine BPTS co-assembled into MTFs [34]. After oxidation, two peaks can be observed with binding energy of 163.4 and 167.9 eV. The second peak is the characteristic of $-SO_3^-$ species [38]. From the integrated areas of S2*p* peaks, almost equal amounts of these two types of sulfur are obtained. These results confirm the proposed mechanism illustrating the incorporation of the gold nanoparticles within MTFs as shown in Scheme 1.

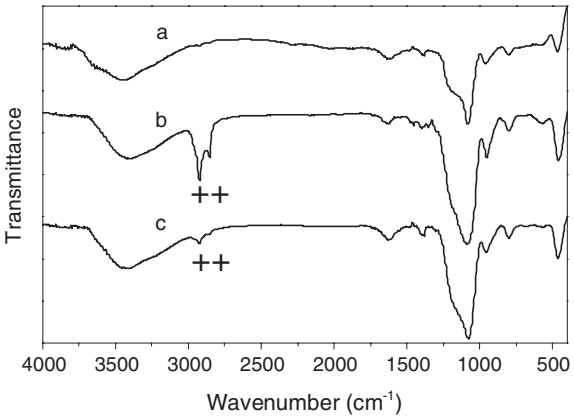

Fig. 1. FT-IR spectra of the MTFs (a) after the removal of Brij56 surfactant of sample S0, (b) as-synthesized sample of S6 and (c) after the removal of Brij56 surfactant of sample S6.

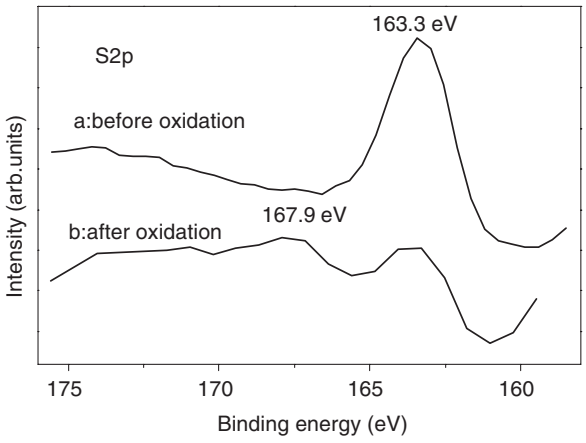

Fig. 2. XPS spectra of sample S4 before (a) and after (b) oxidation with concentrated HNO_3.

Mesostructural and ordered characteristics of the films were manifested by XRD measurements. Curves a, b, c and d in Fig. 3 correspond to the small-angle XRD patterns of S2, S4, S6 and S8 samples before extraction, respectively.

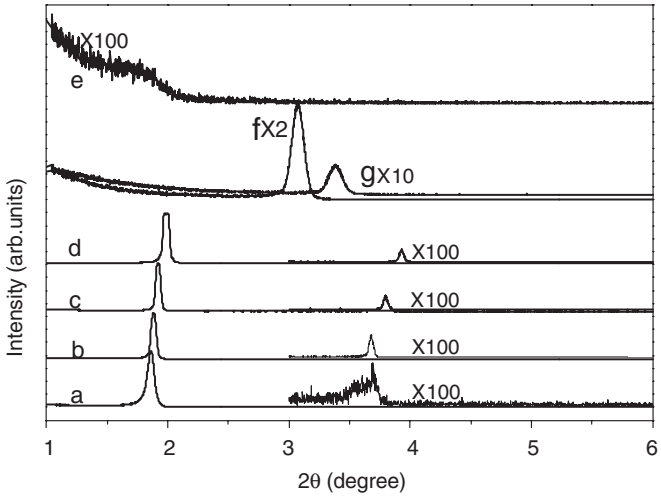

Fig. 3. Small-angle XRD patterns of the as-synthesized (a) S2, (b) S4, (c) S6, (d) S8 and (e) S10 samples; (f) samples S6 after the extraction of Brij56 surfactant, and (g) the gold-loaded composite films from S6 samples.

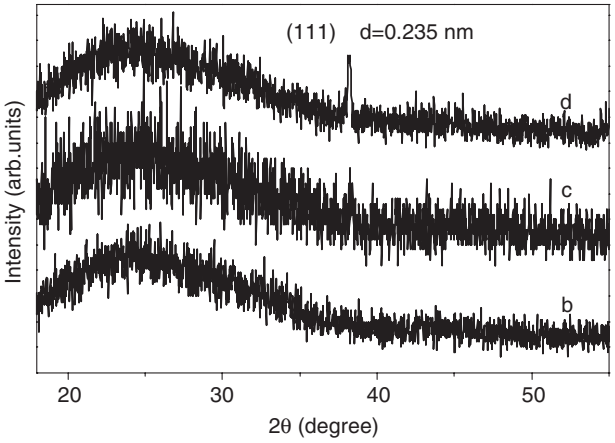

Fig. 4. Wide-angle XRD patterns of gold-loaded composite films from (b) S4, (c) S6 and (d) S8 samples.

They all show a strong and a weak XRD reflection. For S2 sample, two peaks at $2\theta = 1.89$ and 3.79° correspond to d values of 4.7 and 2.3 nm, respectively. With more BPTS organosiloxane being introduced into the framework of MTFs, the reflection peaks shift to higher angle possibly due to the different molecular size of BPTS from that of TEOS, which is in agreement with our previous work [33]. However, when the molar ratio of BPTS:TEOS is up to 10:90 in the starting sol used for the preparation of MTFs, the peak intensity decreases dramatically and broadens, and no second-order peak can be detected as shown in Fig. 3e. This indicates that the structural ordering of the organic and inorganic mesoporous composite films suffer disturbance from higher concentration of BPTS. After the extraction under acid condition for ordered mesoporous composite films, the peaks shift toward the higher angle as shown in Fig. 3f and further shift during the calcination process at 300 °C due to the further contraction of silica framework. An apparent decrease of the small-angle XRD peak intensity can be found after the incorporation of gold nanoparticles, which indicates that gold nanoparticles have been indeed embedded within MTFs and cause the reduction of the peak intensity in consistent with our previous work [5,31].

Curves b, c and d in Fig. 4 show the wide-angle XRD (WAXRD) patterns of the gold/MTFs composite prepared from S4, S6 and S8 samples. For composite films prepared from S8 samples containing more $-SO_3^-$ groups oxidized from thioether moieties, an obvious diffraction peak at $2\theta = 38.2^\circ$ assigned to (111) planes of face-centered cubic (fcc) structure gold is observed, which indicates that gold nanoparticles have well crystallized [5]. The small crystalline grain size can cause the broadened diffraction peak [39]. It should be emphasized that since the films are as thin as ca. 100 nm, the diffraction signals are generally undetectable if the incorporated gold amount within the films is not high enough [26]. When the concentration of $-SO_3^-$ groups reduced, e.g. for composite films prepared from S6, the relative intensity of (111) diffraction peak decreases and the peak shape further broadens. However, no diffraction peak can be observed for those prepared from S4 and S2 samples due to the relatively lower gold contents. These results show that the gold loading level is correlated with the amount of BPTS and controllable since the amount of organosiloxane mixed into the precursor sol for preparing MTFs is readily adjustable.

The morphology and distribution of gold nanoparticles within the MTFs were directly observed by TEM. Fig. 5a, b, c, and d correspond to the composite films prepared from S2, S4, S6 and S8 samples. From Fig. 5, it can be observed that gold nanoparticles as dark dots are well separated from each other and are homogeneously distributed in the mesoporous silica matrix, which results from the molecular level homogeneous dispersion of the co-assembled organosiloxane coupling agent in the silica matrix. The gold nanoparticles are in the size range of 3–7 nm. It should be noted that since the BPTS has both acted as building units of the silica framework and also provided organic surface groups, the gold nanoparticles could penetrate the framework of MTFs and occupy more than one pore/wall period. For composite films prepared from S4 (Fig. 5b), it can be found that the gold loading level increases as compared to those prepared from S2 in Fig. 5a. The sizes of the embedded nanoparticles have also increased slightly due to the more gold precursor of positively charged $Au(en)_2^{3+}$ ions adsorbed by $-SO_3^-$. The more BPTS organosiloxane precursor is mixed into the starting sol for preparing MTFs, the higher gold concentration is obtained as shown in Fig. 5c and d corresponding to S6 and S8 samples. This change trend can also be analyzed via the histograms in the bottom inset of Fig. 5. It is found that mean diameters of gold nanoparticles are statistically around 5.9 and 5.5 nm corresponding to S8 and S6 samples. For S4 and S2 samples, the mean diameters are about 4.7 and 3.9 nm from histograms, respectively. The inset of SAED patterns (top) in Fig. 5a clearly shows that

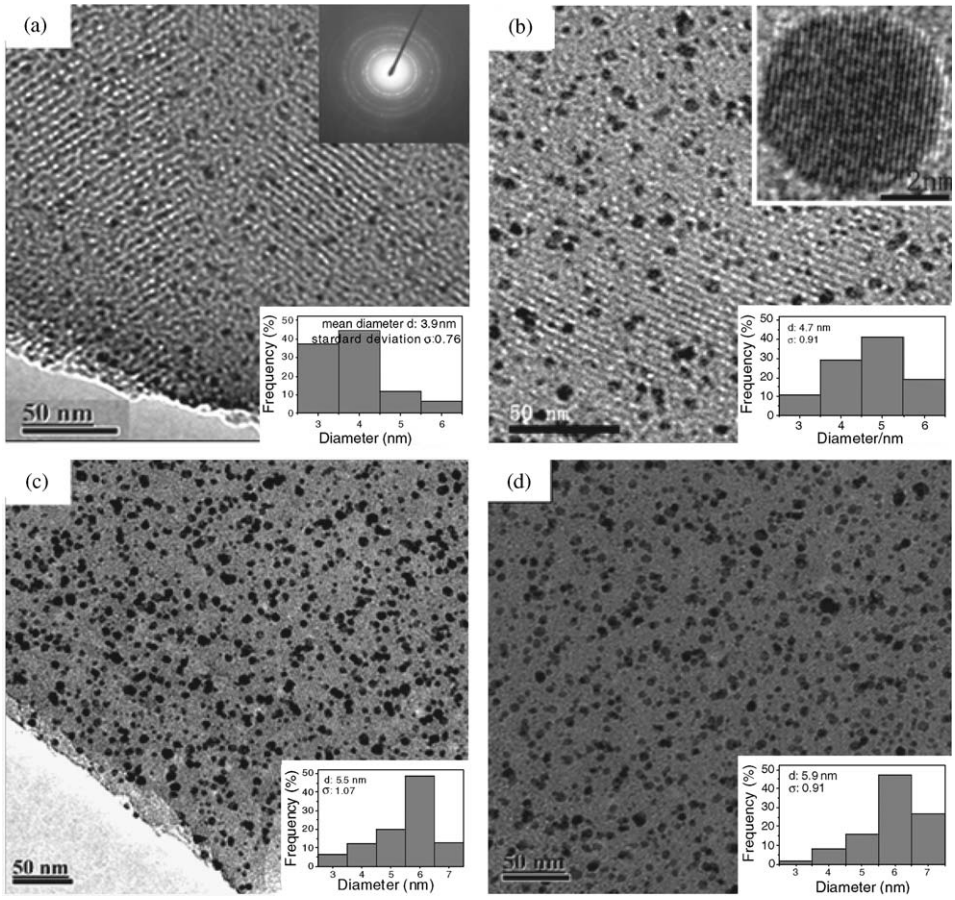

Fig. 5. Typical TEM images of the MTFs embedded with gold nanoparticles from (a) S2, (b) S4, (c) S6, and (d) S8 samples. The inset (top) in Fig. 5a shows the selected area electron diffractions of the composite films and the inset (top) in Fig. 5b shows HRTEM image of a single gold nanoparticle. The insets (bottom) in Fig. 5a, b, c and d show the histograms of the introduced gold nanoparticle size distribution.

the gold nanoparticles have well crystallized. The inset in Fig. 5b shows HRTEM image of a single Au nanoparticle, which demonstrates {111} lattice fringes with an interplanar spacing of ca. 0.24 nm similar to those of fcc gold [39]. The simultaneous EDS of Fig. 6 corresponding to Fig. 5c further indicates the presence of gold within MTFs.

Fig. 7 shows the XPS spectra of Si2*s*, Si2*p* and Au4*f* electron states. The two peaks at 83.7 and 87 eV correspond to the spin doublet of the metallic state Au4$f_{7/2}$ and Au4$f_{5/2}$ [40], which suggests that gold precursor has been effectively reduced under H_2 and N_2 mixing atmosphere at 300 °C. The gold weight content calculated from the integrated areas of Si2*s* peaking at 153.5 eV [41] and Au4*f* is shown in the inset (top) of Fig. 7. It can be seen that the gold loading level increases with the higher ratio of BPTS/TEOS in the starting sol, which is in agreement with the results of WAXRD and TEM observations, and further demonstrates that with our strategy, one can obtain controllable gold concentration within MTFs. The resultant gold weight content is as high as 5.1 wt% for the composite films prepared from S8 samples. For S6, S4, and S2 samples, their weight contents are about 4.3%, 2.8% and 2.1% calculated from the spectra of XPS, respectively.

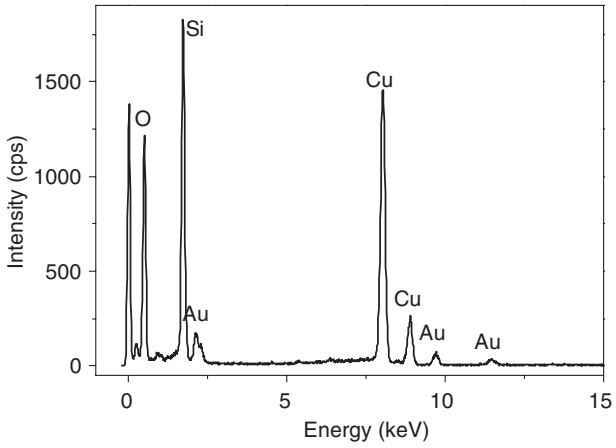

Fig. 6. EDS spectrum of the MTFs embedded with gold nanoparticles corresponding to the region of Fig. 5(c).

Fig. 8 shows the optical absorption spectra of the blank films and the composite films with the Au nanoparticles being incorporated. Though the parent films show no absorption in the wavelength region >400 nm, the composite films containing gold nanoparticles demonstrate an surface plasmon resonance (SPR) absorption peak

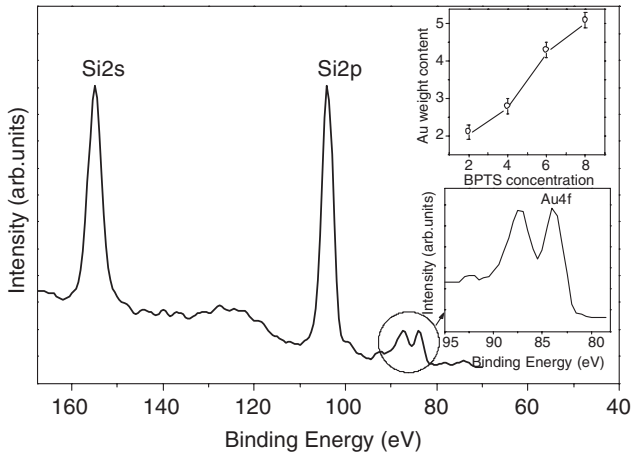

Fig. 7. XPS spectra of Si2*s*, Si2*p* and Au4*f* electrons. The inset (top) shows the gold weight content calculated from the integrated areas from Si2*s* and Au4*f* electrons corresponding to S2, S4, S6 and S8 samples.

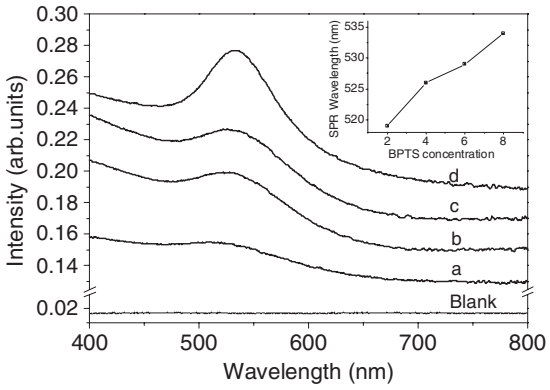

Fig. 8. UV–vis spectra of gold-loaded composite films prepared from (a) S2, (b) S4, (c) S6 and (d) S8 samples. The inset shows the relation of SPR peak position with the BPTS concentration.

along with increased backgrounds, which originate from an interband transition of valence electrons in the *d* band to the Fermi surface [42]. An overall increase in the adsorption intensity can be observed at higher gold loading levels. According to Mie's scattering theory [43,44] in the electric dipole approximation, the absorption coefficient is closely related to the volume fraction of the embedded metal nanoparticles. Therefore, it is believed that the increased relative peak intensity and backgrounds from curve a, b, c to d is due to the relative higher gold loading level. This result further indicates that gold load level within MTFs is controllable dependent on the original BPTS/TEOS ratio in agreement with the results of WAXRD, XPS and TEM characterizations. From the spectra, a red shift of absorption peak together with a comparatively narrower bandwidth can also be found as the gold concentration within the films increase. Generally, the SPR absorption peak position should be at the frequency where $\varepsilon_1(\omega) + 2\varepsilon_m(\omega) = 0$. The peak position and the full-width at half-maximum (FWHM) of SPR depend implicitly on particle size through the dielectric constant of the gold nanoparticles. When the diameters of the incorporated gold nanoparticles are smaller than the mean free path in the bulk metal, the conduction electrons are additionally scattered by the surface [43,45] as shown in our case. Since the size of gold nanoparticles has increased slightly at higher gold loading level as shown in TEM images, the electron-surface scattering possibility will certainly decrease. This results in the decrease of the total electrons collision frequency Γ including the bulk contribution Γ_0 (electron–phonon coupling, impurities, defects, etc.) and surface scattering rate. It has been demonstrated that the Γ correlates directly with the FWHM of SPR of the incorporated gold nanoparticles over wide size ranges between 2 and 20 nm diameter [46]. In addition, dielectric functions $\varepsilon_1(\omega)$ and $\varepsilon_2(\omega)$ also change with different size gold nanoparticles due to the changed electron collision frequency. Therefore, we attribute the red shift and the narrower bandwidth of absorption peaks at higher Au concentration to the quantum confinement effect (or classically, electron-surface scattering) and the changed dielectric function resulted from the increase of gold nanoparticle size [47].

4. Conclusion

Homogeneously distributed BPTS organosiloxane coupling agent has been successfully co-assembled with TEOS to form organic groups functionalized mesoporous composite films. After oxidization, the negatively charged SO_3^- groups obtained could effectively enhance the interaction with cationic complex precursors of $Au(en_2)^{3+}$. Following with calcinations under hydrogen and nitrogen mixing atmosphere, highly dispersed gold nanoparticles loaded MTFs were obtained. The gold content was controllable dependent on the original ratio of BPTS to TEOS. The method can be extended to prepare a variety of other metal and metal oxides nanoparticles via the selection of the different metal ions and calcinations under different atmospheres. The current method will be useful in the preparation of novel electronic and photonic composite films.

Acknowledgments

This work was supported by National Project for Fundamental Research, Grant no. 2002CB613300, National Natural Science Foundation of China, Grant no. 50232050, National Hi-Tech Project of China, Grant no. 2002AA321010, and Shanghai Special Project, Grant no. 03DJ14004.

References

[1] M. Fukushima, H. Yanagi, S. Hayashi, N. Suganuma, Y. Taniguchi, Thin Solid Films 438 (2003) 39.
[2] Y. Hida, H. Kozuka, Thin Solid Films 476 (2005) 264.

[3] W.P. Hu, S.J. Chen, K.T. Huang, J.H. Hsu, W.Y. Chen, G.L. Chang, K.A. Lai, Biosens. Bioelectron. 19 (2004) 1465.
[4] G. Schmid, G.L. Hornyak, Curr. Opin. Solid State Mater. Sci. 2 (1997) 204.
[5] J.L. Gu, J.L. Shi, G.J. You, L.M. Xiong, S.X. Qian, Z.L. Hua, H.R. Chen, Adv. Mater. 17 (2005) 557.
[6] K. Fukumi, A. Chayahara, K. Kadono, T. Sakaguchi, Y. Horino, M. Miya, J. Hayakawa, M. Satou, Jpn. J. Appl. Phys. 30 (1991) L742.
[7] H.B. Liao, R.F. Xiao, H. Wang, K.S. Wong, G.K.L. Wong, Appl. Phys. Lett. 72 (1998) 1817.
[8] S.T. Selvan, T. Hayakava, M. Nogami, Y. Kobayashi, L.M. Liz-Marzan, Y. Hamanaka, A. Nakamura, J. Phys. Chem. B 106 (2002) 10157.
[9] L. Armerao, D. Barreca, G. Bottaro, A. Gasparotto, E. Tondello, M. Ferroni, S. Polozzi, Chem. Mater. 16 (2004) 3331.
[10] T. Yazawa, K. Kadono, H. Tanaka, T. Sakaguchi, S. Tsubota, K. Kuraoka, M. Miya, J. Non-Cryst. Solids 170 (1994) 105.
[11] P. Innocenzi, G. Brusatin, A. Martucci, K. Urabe, Thin Solid Films 279 (1996) 23.
[12] D. Zhao, J. Feng, Q. Huo, N. Melosh, G.H. Fredrickson, B.F. Chmelka, G.D. Stucky, Science 279 (1998) 548.
[13] J.L. Shi, Z.L. Hua, L.X. Zhang, J. Mater. Chem. 14 (2004) 795.
[14] L.X. Zhang, J.L. Shi, J. Yu, Z.L. Hua, X.G. Zhao, M.L. Ruan, Adv. Mater. 14 (2002) 1510.
[15] V. Hornebecq, M. Antonietti, T. Cardinal, M.T. Delapierre, Chem. Mater. 15 (2003) 1993.
[16] H. Zhu, B. Lee, S. Dai, S.H. Overbury, Langmuir 19 (2003) 3974.
[17] Z. Konya, V.F. Puntes, I. Kiricsi, J. Zhu, J.W. Ager III, M.K. Ko, H. Frei, P. Alivisatos, G.A. Somorjai, Chem. Mater. 15 (2003) 1242.
[18] H.R. Chen, J.L. Shi, Y.S. Li, J.N. Yan, Z.L. Hua, H.G. Chen, D.S. Yan, Adv. Mater. 15 (2003) 1078.
[19] S. Cheng, Y. Wei, Q. Feng, K.-Y. Qiu, J.-B. Pang, S.A. Jansen, R. Yin, K. Ong, Chem. Mater. 15 (2003) 1560.
[20] A. Ghosh, C.R. Patra, P. Mukherjee, M. Sastry, R. Kumar, Micro. Meso. Mater. 58 (2003) 201.
[21] N. Liu, R.A. Assink, C.J. Brinker, Chem. Commun. (2003) 370.
[22] J.L. Gu, J.L. Shi, L.M. Xiong, H.R. Chen, M.L. Ruan, Micro. Meso. Mater. 74 (2004) 119.
[23] Ö. Dag, O. Samarskaya, N. Coombs, G.A. Ozin, J. Mater. Chem. 13 (2003) 328.
[24] S. Besson, T. Gacoin, C. Ricolleau, J.P. Boilot, Chem. Commun. (2003) 360.
[25] Y. Plyuto, J.M. Berquier, C. Jacquiod, C. Ricolleau, Chem. Commun. (1999) 1653.
[26] A. Fukuoka, H. Araki, Y. Sakamoto, N. Sugimoto, H. Tsukada, Y. Kumai, Y. Akimoto, M. Ichikawa, Nano Lett. 2 (2002) 793.
[27] A. Fukuoka, H. Araki, J. Kimura, Y. Sakamoto, T. Higuchi, N. Sugimoto, S. Inagaki, M. Ichikawa, J. Mater. Chem. 14 (2004) 752.
[28] C. Yang, H. Shen, K. Chao, Adv. Funct. Mater. 12 (2002) 143.
[29] C. Yang, P. Liu, Y. Ho, C. Chiu, K. Chao, Chem. Mater. 14 (2002) 275.
[30] S. Huh, J.W. Wiench, J.C. Yoo, M. Pruski, V.S.Y. Lin, Chem. Mater. 15 (2003) 4247.
[31] X.G. Zhao, J.L. Shi, B. Hu, L.X. Zhang, Z.L. Hua, J. Mater. Chem. 13 (2003) 399.
[32] A. Sayari, S. Hamoudi, Chem. Mater. 13 (2001) 3151.
[33] L.X. Zhang, W.H. Zhang, J.L. Shi, Z.L. Hua, Y.S. Li, J.N. Yan, Chem. Commun. (2003) 210.
[34] Y. Guo, A.R. Guadalupe, O. Resto, L.F. Fonseca, S.Z. Weisz, Chem. Mater. 11 (1999) 135.
[35] F. Cagnol, D. Crosso, C. Sanchez, Chem. Commun. (2004) 1742.
[36] M. Epifani, E. Carlino, C. Blasi, C. Giannini, L. Tapfer, L. Vasanelli, Chem. Mater. 13 (2001) 1533.
[37] B.P. Block, J.C. Bailar, J. Am. Chem. Soc. 73 (1951) 4722.
[38] S. Chatarvedi, J.A. Rodriguez, J. Hrbek, J. Phys. Chem. B 101 (1997) 10860.
[39] J.L. Gu, J.L. Shi, H.R. Chen, L.M. Xiong, L. Li, M.L. Ruan, Solid State Sci. 6 (2004) 747.
[40] T. Ishizaka, S. Muto, Y. Kurokawa, Opt. Commun. 190 (2001) 385.
[41] A. Azioune, A.B. Slimane, L.A. Hamou, A. Pleuvy, M.M. Chehimi, C. Perruchot, S.P. Armes, Langmuir 20 (2004) 3350.
[42] H. Inouye, K. Tanaka, I. Tanahashi, K. Hirao, Phys. Rev. B 57 (1998) 11334.
[43] J.H. Hodak, A. Henglein, G.V. Hartland, J. Phys. Chem. B 104 (2000) 9954.
[44] M.M. Alvarez, J.T. Khoury, T.G. Schaaff, M.N. Shafigullin, I. Vezmar, R.L. Whetten, J. Phys. Chem. B 101 (1997) 3706.
[45] R.H. Magruder III, L. Yang, R.F. Haglund Jr., C.W. White, L. Yang, R. Dorsinville, R.R. Alfano, Appl. Phys. Lett. 62 (1993) 1730.
[46] H. Hövel, S. Fritz, A. Hilger, U. Kreibig, M. Vollmer, Phys. Rev. B 48 (1993) 18178.
[47] R.D. Averitt, D. Sarkar, N.J. Halas, Phys. Rev. Lett. 78 (1997) 4217.